Impact of Spectators on a Two-Qubit Gate in a Tunable Coupling Superconducting Circuit

T.-Q. Cai, X.-Y. Han, Y.-K. Wu, Y.-L. Ma, J.-H. Wang, Z.-L. Wang, H.-Y Zhang, H.-Y Wang, Y.-P. Song,* and L.-M. Duan†

Center for Quantum Information, Institute for Interdisciplinary Information Sciences, Tsinghua University, Beijing 100084, China

(Received 20 February 2021; accepted 6 July 2021; published 5 August 2021)

Cross-resonance (CR) gates have emerged as a promising scheme for fault-tolerant quantum computation with fixed-frequency qubits. We experimentally implement an entangling CR gate by using a microwave-only control in a tunable coupling superconducting circuit, where the tunable coupler provides extra degrees of freedom to verify optimal conditions for constructing a CR gate. By developing a three-qubit Hamiltonian tomography protocol, we systematically investigate the dependency of gate fidelities on spurious qubit interactions and present the first experimental approach to the evaluation of the perturbation impact arising from spectator qubits. Our results reveal that the spectator qubits lead to reductions in CR gate fidelity dependent on ZZ interactions and particular frequency detunings between spectator and gate qubits. The target spectator demonstrates a more serious impact than the control spectator under a standard echo pulse scheme, whereas the degradation of gate fidelity is observed up to 22.5% as both the spectators are present with a modest ZZ coupling to the computational qubits. Our experiments uncover an optimal CR operation regime, and the method we develop here can readily be applied to improving other kinds of two-qubit gates in large-scale quantum circuits.

DOI: 10.1103/PhysRevLett.127.060505

In complex superconducting circuits with larger numbers of qubits [1–5], the fidelity of quantum algorithms begins to be dominated by unwanted qubit interactions, increased decoherence, and frequency crowding, all inherent to traditional frequency-tuned architectures [6–9]. Alternatively, a microwave-only control scheme like cross-resonance (CR) gates can provide frequency selectivity and allow one to use fixed-frequency computational qubits, thereby minimizing the sensitivity of the qubits with respect to the sources of possible noise [10,11]. The CR gate scheme [12–17] has a strong appeal to the multiqubit control in superconducting architectures using fixed-frequency transmon qubits, thus allowing the qubits to be operated at their optimal bias points for coherence; also, it only requires a single microwave drive line for applying the drive tone to the control qubit and thereby efficiently reduces the circuit complexity.

A fast two-qubit CR gate relies on a large coupling that leads to cross talk between qubits [12,15]. In practice, the computational qubits of a CR gate cannot be efficiently isolated from the environment and are inevitably exposed to neighboring qubits owing to mutual interactions in a quantum processor [18,19]. A recent theoretical study on CR gates reveals detrimental multiqubit frequency collisions as a control or target qubit couples to a third spectator qubit [20], thus leading to a reduction in gate fidelity. To eliminate this deadly impact, it becomes crucial to study the dependency of the unwanted components on the coupling between the qubits. In particular, what is needed is an experimental investigation of an optimal CR gate operation regime in the presence of spectator qubits. These key issues, however, have not yet been explored due to a lack of control of the interactions between the qubits. Fortunately, the experimental realization of tunable couplers provides a way to adjust qubit interactions and hence offers a possibility for mitigating unwanted couplings [21–26].

In this Letter, exploiting flux-controlled tunable couplers, we address these crucial barriers to optimizing CR gate control by systematically investigating the dependency of gate fidelities on spurious interaction components. We present the first experimental approach to the evaluation of the perturbation impact arising from the spectator qubits, providing a guiding principle to improve two-qubit gate fidelity with spectator qubits for large-scale quantum computation.

Experimental setup and isolated CR gate.—Our quantum processor consists of seven transmon qubits ($Q_i, i = 1$–7) with each pair of neighboring qubits mediated via a frequency-tunable coupler ($C_j, j = 1$–6). In our experiments, the qubits Q_i ($i = 2, 3$) and Q_i ($i = 1, 4$), as outlined in Fig. 1(a), are used to implement the CR gate as the computational gate qubits and spectator qubits, respectively. We schematically represent our experimental scheme in Fig. 1(b). A cross drive on the control qubit,

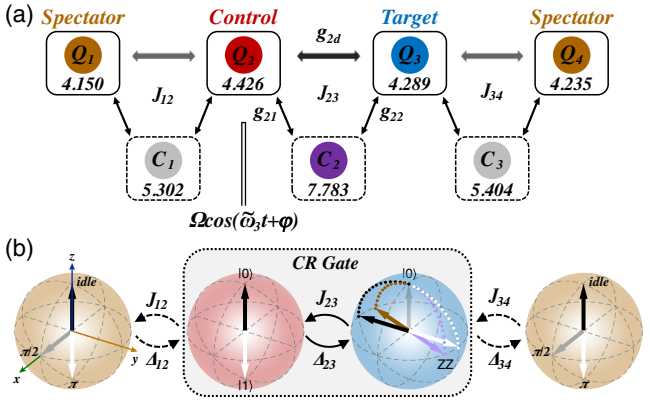

FIG. 1. (a) Sketch of the experimental subsystem. The qubit frequencies (in GHz) are displayed in the corresponding boxes. The two computational qubits are coupled with an effective coupling J_{23} via a direct coupling with strength g_{2d} and indirect couplings through the coupler with g_{21} and g_{22}, respectively. (b) Schematic representation of the experimental scheme. The black (white) and brown (purple) dots depict ideal and distorted state trajectories of the target qubit on a Bloch sphere, respectively. The distortion is due to the impact of the ZZ interaction from the target spectator.

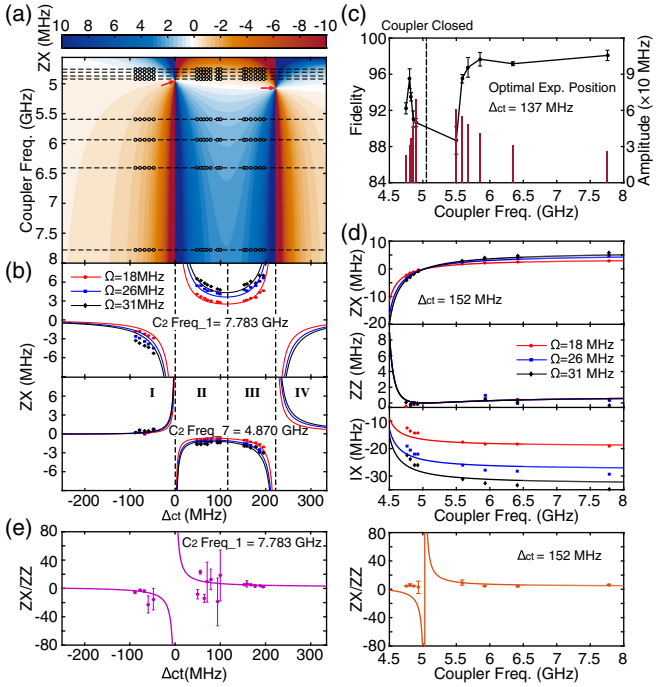

FIG. 2. (a) Numerical simulations and measurements of ZX interaction with the fixed CR drive amplitude $\Omega = 18$ MHz. (b) Cross-sectional views of (a) at two representative coupler frequencies with three sets of CR drive amplitudes. (c) Change in the quantum process tomography (QPT) fidelity (black dot) as a function of the coupler qubit frequency (left axis). The corresponding CR drive amplitudes (dark red narrow bar) used for acquiring the QPT fidelities (right axis). (d) ZX, ZZ, and IX vary as a function of the coupler (C_2) frequency with three different CR drive amplitudes. (e) The experimental (dots) and numerical (solid lines) results of the ZX/ZZ ratio vary with the qubit frequency detuning Δ_{ct} (left panel) and the coupler (C_2) frequency (right panel). The optimal operating condition is expected in the region where the ZX/ZZ ratio is large but insensitive to the coupler frequency.

at the target qubit frequency, rotates the target either around the $+x$ axis or $-x$ axis, depending on the state of the control. By contrast, the presence of spectator qubits distorts the quantum trajectory of the target and hence degrades the two-qubit gate performance. By developing three-qubit Hamiltonian tomography, intriguingly, we can extract all unwanted interactions and reveal an optimal gate operation regime.

We first consider an isolated CR gate. Both gate qubits are negatively detuned from the coupler $\Delta_i = \omega_i - \omega_c < 0$ $(i = 2,\ 3)$, where $\omega_{2,3}$, ω_c are the frequencies of Q_2, Q_3, and C_2, respectively. We apply a CR drive pulse $\Omega\cos(\omega_d t + \phi)$ on the control qubit Q_2 with an amplitude Ω, frequency ω_d, and phase ϕ. When the qubit drive is present, the system Hamiltonian is

$$H/\hbar = \sum_{i=2,3} \frac{1}{2}\tilde{\omega}_i \sigma_i^z + J_{23}(\sigma_2^+\sigma_3^- + \sigma_3^+\sigma_2^-) + \Omega\cos(\omega_d t + \phi)\sigma_2^x, \quad (1)$$

where σ_α^x, σ_α^z, σ_α^+, σ_α^- $(\alpha = 2, 3)$ are the Pauli X, Pauli Z, and raising and lowering operators for Q_2 and Q_3, respectively; $\tilde{\omega}_2 = \omega_2 + (J_{23}/\Delta)$, $\tilde{\omega}_3 = \omega_3 - (J_{23}/\Delta)$, $J_{23} = g_{2d} + (g_{21}g_{22}/\Delta)$, $(1/\Delta) = [(1/\Delta_2) + (1/\Delta_3)]/2$ [27–30]. On the condition that $\Omega, J_{23} \ll \Delta$ and the drive frequency ω_d is in resonance with the target qubit (Q_3) frequency $\tilde{\omega}_3$, considering cross talks on the processor chip and off-resonance drive on the control qubit, the effective drive Hamiltonian can be expressed as $H_{\rm eff}/\hbar = u_1 ZX + u_2 ZY + u_3 ZZ + u_4 ZI + u_5 IX + u_6 IY + u_7 IZ$ [15,31]. The first one is the CR term, while the rest are the unwanted residual qubit interaction terms in the gate operation.

To verify optimal implementation parameters and extract error terms in the gate operation, we numerically calculate CR Hamiltonian components based on the lowest-order energy-basis representation method [20] with experimental parameters. We plot the primary interaction term ZX as a function of control-target qubit frequency detuning Δ_{ct} and coupler frequency, as shown in Fig. 2(a). The results reveal that the interaction component is sensitive to the frequency detuning, featuring two-qubit resonance poles where the interaction value becomes infinite as the detuning crosses the gate parameters $\Delta_{\rm ct} = 0$, $\Delta_{\rm ct} = \pm\alpha_i = \pm 222$ MHz $(i = 2,\ 3)$, and thus divides the gate operation into the distinct regions labeled I, II, III, and IV. Moreover, the interaction term undergoes the turning points (indicated by red arrows) that are slightly dependent on the frequency detuning, as the coupler frequency passes across the

transition point. We experimentally measure the CR Hamiltonian and fit Rabi oscillations with a Bloch equation model function [15], using the pulse sequence sketched in the Supplemental Material [32–38]. The measured ZX interaction at eight different coupler frequencies, as shown in Fig. 2(a), is displayed in black circles with color intensity inside to identify the interaction strengths, which are consistent with the numerical calculations. To highlight its dependence on the frequency detuning, we plot the measured ZX and the simulated ZX (solid lines) in Fig. 2(b). The aforementioned distinct regions are clearly distinguished with the detuning transitions. Furthermore, we selectively plot three interaction components of both the measured and the calculated ZX, ZZ, and IX in Fig. 2(d) as a function of the coupler frequency with three different drive amplitudes and a fixed $\Delta_{\mathrm{ct}} = 152$ MHz. We find that the large ZX rate and the relatively small static ZZ interaction in region III define an optimal operating regime in our experiment, which is confirmed by the experimental data and numerical calculations (solid lines) shown in the left panel of Fig. 2(e). In addition, the right panel of Fig. 2(e) implies that ZX/ZZ is less sensitive to the coupler frequency except for the region near $ZZ = 0$.

To suppress the unwanted CR components, we verify an appropriate CR drive phase, and perform CR Rabi experiments by using an echo scheme [15,39]. The state trajectory of the target qubit is depicted in a Bloch sphere in Fig. S6(g) in the Supplemental Material during the CR gate operation, showing a near perfect circle on the surface of the Bloch sphere, which confirms that the echo scheme improves the gate evolution. According to the results shown in Figs. 2(b) and 2(e), and taking into account the qubit coherence time at the selected frequency, we measure the quantum process tomography (QPT) gate fidelity at $\Delta_{ct} = 137$ MHz by varying the coupler qubit frequency. As shown in Fig. 2(c), the QPT fidelity maximizes at a coupler frequency of 7.783 GHz, and a deep valley of fidelity emerges in a coupler frequency region between 4.8 and 5.6 GHz. Figure S6(f) in the Supplemental Material [32] shows the χ_{exp} and χ_{ideal} for the CR entangling gate acquired under the optimal operating position, demonstrating a 98.5% gate fidelity from the maximum-likelihood estimation, primarily limited by qubit decoherence [40].

CR gate with spectator qubits.—In order to identify a more realistic scenario of gate operation, we construct a CR gate with a third spectator qubit that couples to the control or the target qubit. We implement three-qubit Hamiltonian tomography to distinguish the various interaction components in the gate operation. We consider that both the spectator and the control qubits only contribute $\{I, Z\}$ interactions to the effective Hamiltonian, while the target qubit involves all Pauli interactions $\{I, X, Y, Z\}$ and others due to the off-resonance drive on the control qubit [20]. Hence, the gate operators with a control spectator qubit can

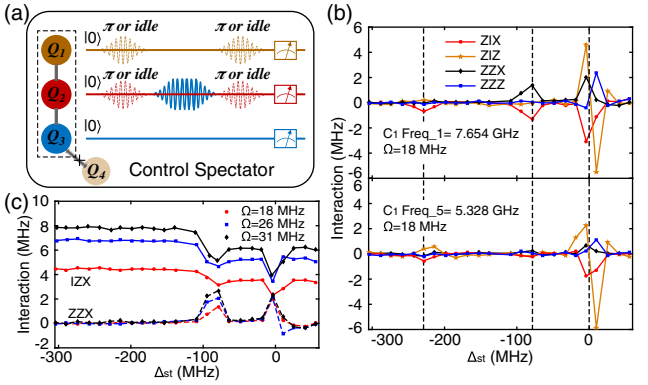

FIG. 3. (a) Schematic pulse sequence for measuring three-qubit Hamiltonian tomography with a control spectator qubit. The π pulses (dashed line) or idle pulses (no pulse) consequently applied on Q_1 and Q_2 before and after the CR pulse (solid line) generate a fourfold spectator-control subspace of $|00\rangle$, $|01\rangle$, $|10\rangle$, and $|11\rangle$. (b) The dominant interaction terms, in the control spectator case, vary as a function of Δ_{st} with two fixed coupler (C_1) frequencies and a CR drive amplitude at 18 MHz. All interaction terms demonstrate extreme changes in certain detuning regions ($\Delta_{st} = 0, -85, -222$ MHz). (c) Three-qubit IZX and ZZX terms vary with Δ_{st} and CR drive amplitude in the control spectator case.

be defined as $|\mathrm{spectator}\rangle \otimes |\mathrm{control}\rangle \otimes |\mathrm{target}\rangle = \{I, Z\} \otimes \{I, Z\} \otimes \{I, X, Y, Z\}$. We experimentally measure the three-qubit Hamiltonian tomography to extract primary interaction terms using the schematic pulse sequence depicted in Fig. 3(a). This is accomplished by turning on the CR drive for some time and then measuring the Rabi oscillations on the target qubit in the spectator $\otimes$ control subspace of $|00\rangle, |01\rangle, |10\rangle, |11\rangle$ for projecting the target qubit state onto the x, y, and z axes. Similar to the approach developed for the two-qubit Hamiltonian tomography [15], the Rabi oscillations can be fitted with a Bloch equation model function: $\dot{\vec{r}}_{\{00,01,10,11\}}(t) = e^{Gt}\vec{r}_{\{00,01,10,11\}}(0), (r = x, y, z)$. $\vec{r}(t)$ is the vector composed of three projecting measurement values, $\langle x(t)\rangle$, $\langle y(t)\rangle$, $\langle z(t)\rangle$, as a function of the length of the Rabi drive. G is a matrix defined in Eq. (S3) in the Supplemental Material [32].

We separately extract the three-qubit CR drive Hamiltonian terms by changing the coupling strength J_{12} between Q_1 and Q_2 and the frequency detuning Δ_{st} between Q_1 and Q_3. Figure 3(b) displays the primary three-qubit gate parameters as a function of Δ_{st}. Apparently, in certain resonance regions, unwanted energy excitations occur, breaking down the CR gate regime. For instance, the condition of $\Delta_{\mathrm{st}} = 0$ leads to a resonance between $|100\rangle$ and $|001\rangle$, while the parameters in the region around $\Delta_{\mathrm{st}} = -85$ MHz result in a resonance of $|110\rangle$ and $|020\rangle$. Except for these regions, the interaction terms remain almost intact with different coupling strengths. The interaction terms, such as ZIX, ZZX, ZIZ, and ZZZ,

describe the effective mediated interaction between the control spectator Q_1 and the target qubit Q_3 through the control qubit Q_2. These terms affect the evolution of the target qubit and thus degrade the CR gate fidelity. Moreover, these three-qubit Hamiltonian interaction terms also have a dependence on the CR drive amplitude. As an example, the ZZX and IZX interactions, illustrated in Fig. 3(c), are enhanced with an increase in CR drive amplitude, which is more pronounced in the resonance pole region for the ZZX term.

Similarly, we can conduct three-qubit CR Hamiltonian tomography with a target spectator qubit. Compared to the perturbation impact from the control spectator qubit, we find that the target spectator qubit affects the CR gate more seriously as Δ_{st} is close to the resonance poles due to the stronger unwanted energy excitations. In fact, a slight jitter of the target qubit frequency from the static ZZ interaction between Q_3 and Q_4 or the unwanted energy resonance at $\Delta_{st} = 0$ between $|001\rangle$ and $|010\rangle$, as an example, will seriously disturb or even break down the CR gate operation where the target qubit undertakes the main evolution process, whereas the control qubit is not directly excited.

Impact of spectator qubits on CR gate fidelity.—We first investigate the CR gate fidelity susceptible to the frequency detunings between the spectators and the target qubit. We extract the ZZ interaction between Q_1 and Q_2 (Q_3 and Q_4) via a Ramsey-type experiment that involves probing the frequency of one qubit with another in either its ground or excited state [41,42]. To probe the perturbation impact in various conditions, we execute multiple sets of QPT experiments for each operation point, selectively applying a π or $\pi/2$ pulse on Q_1 or Q_4, respectively. The QPT measurement with idle pulse (no pulse) on the spectator qubits (in ground state) sets a control fidelity for each operation point with the particular coupling condition for comparison with the measurements with pulse applied on the spectator qubits (experimental fidelity). The relative gate error in Fig. 4, defined as the difference between the experimental fidelity and the control fidelity, reflects the perturbation impact from the spectator qubits. We observe larger relative gate errors or even failure of the gate, as shown in Figs. 4(b) and 4(c), near the frequency resonance poles indicated by dashed lines, especially in the target spectator case, revealing that unwanted energy excitations play a major role in degrading the CR gate fidelity. Away from the resonance poles, the gate error, however, relies more on the ZZ interaction, demonstrating certain positive correlations—for instance, among the data points in the control spectator case, where the spectator does not cause a deadly impact as the target spectator does.

We then explore the CR gate fidelity dependent on the coupling strength between the spectators and the gate qubits in three operation regions by modifying the frequency of C_1 and C_3 (see the Supplemental Material [32]). As expected, the spectator qubits have almost no

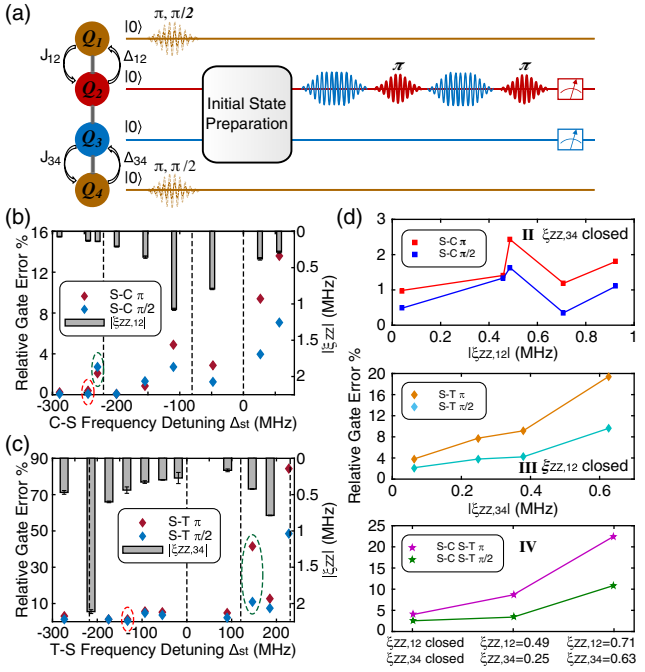

FIG. 4. (a) Schematic pulse sequence for investigating the CR gate fidelity with spectator qubits. We categorize the operation into four regions: I: both couplings (J_{12} and J_{34}) off; II: J_{12} coupling on while J_{34} off; III: J_{12} off while J_{34} on; IV: both J_{12} and J_{34} on. (b),(c) The relative QPT gate error and ZZ interaction (with error bar) vs the frequency detuning of the spectator Q_1 and Q_4 to the target qubit Q_3 in the control spectator case and the target spectator case, respectively. The CR gate fidelity is subject not only to the ZZ interaction but also to the unwanted energy excitations. The representative data points indicated by red and green dashed ellipse highlight the difference in the impact from the spectators between the regions away and near the frequency resonance poles. (d) The relative QPT gate error vs the ZZ coupling strength between the spectator qubits and the gate qubits in the operation regions II (top panel), III (middle panel), and IV (bottom panel).

perturbation impact on the gate qubit regardless of the operations of the spectator qubits, as the couplings between the gate qubits and the spectator qubits are turned off (region I). Once the coupling is on, however, the perturbation impact obviously occurs, and the relative gate error increases as the magnitude of the ZZ interaction rises, as shown in Fig. 4(d). Particularly, the gate qubits are more susceptible to the perturbation impact from the target spectator qubit (region III) than that from the control spectator qubit (region II). This susceptibility can be attributed to the fact that the standard echo scheme can only effectively reduce errors caused by control spectators [43]. The perturbation impact becomes more serious, evidenced by the larger relative gate error of up to 22.5% when both couplings (J_{12} and J_{34}) are all on (region IV). The rotary pulse scheme developed in Ref. [43] can further reduce the unwanted interactions from the target

spectator with complex rotary pulse control. Note that, near the frequency resonance poles, either the echo pulse scheme or the target rotary protocol will fail due to the fact that the severe leakage from unwanted energy excitations becomes the dominant error source.

Discussions.—The tunable coupling architecture itself provides an extra degree of freedom to tune interactions between computational qubits in an isolated system and thus demonstrates an improvement of the two-qubit gate by verifying an optimal condition via adjusting flux bias on the coupler. However, in a large superconducting network, where one qubit could be treated as a gate qubit in one network block but practically behaves as a spectator qubit in another. To yield a high gate fidelity, the qubit frequencies and coupling strength should be deliberately designed [44] to reach a balance between high CR gate fidelity and feasibility of gate operation. Using flux-controlled tunable couplers in a large-scale superconducting circuit, it is practical to effectively eliminate the impact from both control spectator and target spectator by tuning off the coupling between the spectators and the vulnerable computational subsystem. Yet even in the case where a tunable coupler is unavailable in the circuit, and the gate operation thus suffers from the inevitable spectator perturbation, our result sheds light on a feasible two-qubit gate operation regime by avoiding the resonance pole regions.

In summary, we exploit the flux-controlled tunable coupler to verify the optimal CR operation regime and provide insight into an improvement of two-qubit gates in large-scale quantum circuits. We here emphasize our main conclusions: (1) Our experimental results reveal that the spectator qubits have a significant impact on the computational gate qubits, and the target spectator qubit leads to more serious degradation of the CR gate fidelity than the control spectator qubit under the echo pulse scheme. (2) We systematically investigate the dependency of gate fidelities on spurious interaction components, and the dominant interaction terms are more pronounced in the resonance pole regions. (3) The three-qubit Hamiltonian tomography method we develop here can be extended and applied to other multibody systems for improving the fidelity of two-qubit gates. Our experimental outcomes will be highly desirable as spectator qubits are inevitably presented in large-scale superconducting circuits for fault-tolerant quantum computation [45,46].

We acknowledge Luyan Sun for sharing JPA fabrication parameters. This work was supported by the National Natural Science Foundation of China under Grant No. 11874235, the State's Key Project of Research and Development Plan under Grant No. 2016YFA0301902, and the Tsinghua University Initiative Scientific Research Program.

T.-Q. C. and X.-Y. H. contributed equally to this work.

*Corresponding author.
ypsong@mail.tsinghua.edu.cn
†Corresponding author.
lmduan@tsinghua.edu.cn

[1] M. H. Devoret and R. J. Schoelkopf, Superconducting circuits for quantum information: An outlook, Science **339**, 1169 (2013).
[2] J. Q. You and F. Nori, Atomic physics and quantum optics using superconducting circuits, Nature (London) **474**, 589 (2011).
[3] X. Gu, A. F. Kockum, A. Miranowicz, Y. xi Liu, and F. Nori, Microwave photonics with superconducting quantum circuits, Phys. Rep. **718–719**, 1 (2017).
[4] J. Kelly *et al.*, State preservation by repetitive error detection in a superconducting quantum circuit, Nature (London) **519**, 66 (2015).
[5] R. Barends, J. Kelly, A. Megrant, D. Sank, E. Jeffrey, Y. Chen, Y. Yin, B. Chiaro, J. Mutus, C. Neill, P. O'Malley, P. Roushan, J. Wenner, T. C. White, A. N. Cleland, and J. M. Martinis, Coherent Josephson Qubit Suitable for Scalable Quantum Integrated Circuits, Phys. Rev. Lett. **111**, 080502 (2013).
[6] C. Song, K. Xu, H. Li, Y.-R. Zhang, X. Zhang, W. Liu, Q. Guo, Z. Wang, W. Ren, J. Hao *et al.*, Generation of multicomponent atomic schrödinger cat states of up to 20 qubits, Science **365**, 574 (2019).
[7] A. A. Houck, H. E. Türeci, and J. Koch, On-chip quantum simulation with superconducting circuits, Nat. Phys. **8**, 292 (2012).
[8] C. Neill, P. Roushan, K. Kechedzhi, S. Boixo, S. V. Isakov, V. N. Smelyanskiy, A. Megrant, B. Chiaro, A. Dunsworth, K. Arya *et al.*, A blueprint for demonstrating quantum supremacy with superconducting qubits, Science **360**, 195 (2018).
[9] R. A. Pinto, A. N. Korotkov, M. R. Geller, V. S. Shumeiko, and J. M. Martinis, Analysis of a tunable coupler for superconducting phase qubits, Phys. Rev. B **82**, 104522 (2010).
[10] S. Poletto, J. M. Gambetta, S. T. Merkel, J. A. Smolin, J. M. Chow, A. D. Córcoles, G. A. Keefe, M. B. Rothwell, J. R. Rozen, D. W. Abraham, C. Rigetti, and M. Steffen, Entanglement of Two Superconducting Qubits in a Waveguide Cavity Via Monochromatic Two-Photon Excitation, Phys. Rev. Lett. **109**, 240505 (2012).
[11] J. M. Chow, J. M. Gambetta, A. W. Cross, S. T. Merkel, C. Rigetti, and M. Steffen, Microwave-activated conditional-phase gate for superconducting qubits, New J. Phys. **15**, 115012 (2013).
[12] J. M. Chow, A. D. Córcoles, J. M. Gambetta, C. Rigetti, B. R. Johnson, J. A. Smolin, J. R. Rozen, G. A. Keefe, M. B. Rothwell, M. B. Ketchen, and M. Steffen, Simple All-Microwave Entangling Gate for Fixed-Frequency Superconducting Qubits, Phys. Rev. Lett. **107**, 080502 (2011).
[13] C. Rigetti and M. Devoret, Fully microwave-tunable universal gates in superconducting qubits with linear couplings and fixed transition frequencies, Phys. Rev. B **81**, 134507 (2010).
[14] J. C. Pommerening, Multiqubit Coupling Dynamics and the Cross-Resonance Gate, Ph.D. thesis, RWTH Aachen University, 2017.

[15] S. Sheldon, E. Magesan, J. M. Chow, and J. M. Gambetta, Procedure for systematically tuning up cross-talk in the cross-resonance gate, Phys. Rev. A **93**, 060302(R) (2016).
[16] M. E. Ware, Flux-tunable superconducting transmons for quantum information processing, Ph.D. thesis, Syracuse University, 2015.
[17] S. Kirchhoff, T. Keßler, P. J. Liebermann, E. Assémat, S. Machnes, F. Motzoi, and F. K. Wilhelm, Optimized cross-resonance gate for coupled transmon systems, Phys. Rev. A **97**, 042348 (2018).
[18] F. Arute, K. Arya, R. Babbush, D. Bacon, J. C. Bardin, R. Barends, R. Biswas, S. Boixo, F. G. S. L. Brandao, D. A. Buell *et al.*, Quantum supremacy using a programmable superconducting processor, Nature (London) **574**, 505 (2019).
[19] M. S. Blok, V. V. Ramasesh, T. Schuster, K. O'Brien, J. M. Kreikebaum, D. Dahlen, A. Morvan, B. Yoshida, N. Y. Yao, and I. Siddiqi, Quantum Information Scrambling on a Superconducting Qutrit Processor, Phys. Rev. X **11**, 021010 (2021).
[20] M. Malekakhlagh, E. Magesan, and D. C. McKay, First-principles analysis of cross-resonance gate operation, Phys. Rev. A **102**, 042605 (2020).
[21] P. Mundada, G. Zhang, T. Hazard, and A. Houck, Suppression of qubit crosstalk in a tunable coupling superconducting circuit, Phys. Rev. Applied **12**, 054023 (2019).
[22] X. Li, T. Cai, H. Yan, Z. Wang, X. Pan, Y. Ma, W. Cai, J. Han, Z. Hua, X. Han, Y. Wu, H. Zhang, H. Wang, Y. Song, L. Duan, and L. Sun, Tunable coupler for realizing a controlled-phase gate with dynamically decoupled regime in a superconducting circuit, Phys. Rev. Applied **14**, 024070 (2020).
[23] X. Y. Han, T. Q. Cai, X. G. Li, Y. K. Wu, Y. W. Ma, Y. L. Ma, J. H. Wang, H. Y. Zhang, Y. P. Song, and L. M. Duan, Error analysis in suppression of unwanted qubit interactions for a parametric gate in a tunable superconducting circuit, Phys. Rev. A **102**, 022619 (2020).
[24] R. C. Bialczak, M. Ansmann, M. Hofheinz, M. Lenander, E. Lucero, M. Neeley, A. D. O'Connell, D. Sank, H. Wang, M. Weides *et al.*, Fast Tunable Coupler for Superconducting Qubits, Phys. Rev. Lett. **106**, 060501 (2011).
[25] Y. Chen, C. Neill, P. Roushan, N. Leung, M. Fang, R. Barends, J. Kelly, B. Campbell, Z. Chen, B. Chiaro *et al.*, Qubit Architecture with High Coherence and Fast Tunable Coupling, Phys. Rev. Lett. **113**, 220502 (2014).
[26] D. C. McKay, S. Filipp, A. Mezzacapo, E. Magesan, J. M. Chow, and J. M. Gambetta, Universal gate for fixed-frequency qubits via a tunable bus, Phys. Rev. Applied **6**, 064007 (2016).
[27] A. Blais, J. Gambetta, A. Wallraff, D. I. Schuster, S. M. Girvin, M. H. Devoret, and R. J. Schoelkopf, Quantum-information processing with circuit quantum electrodynamics, Phys. Rev. A **75**, 032329 (2007).
[28] S. Bravyi, D. P. DiVincenzo, and D. Loss, Schrieffer–wolff transformation for quantum many-body systems, Ann. Phys. (Amsterdam) **326**, 2793 (2011).
[29] F. Yan, P. Krantz, Y. Sung, M. Kjaergaard, D. L. Campbell, T. P. Orlando, S. Gustavsson, and W. D. Oliver, Tunable coupling scheme for implementing high-fidelity two-qubit gates, Phys. Rev. Applied **10**, 054062 (2018).
[30] G. Zhu, D. G. Ferguson, V. E. Manucharyan, and J. Koch, Circuit QED with fluxonium qubits: Theory of the dispersive regime, Phys. Rev. B **87**, 024510 (2013).
[31] E. Magesan and J. M. Gambetta, Effective Hamiltonian models of the cross-resonance gate, Phys. Rev. A **101**, 052308 (2020).
[32] See Supplemental Material at http://link.aps.org/supplemental/10.1103/PhysRevLett.127.060505 for the theory of Hamiltonian tomography, sample and measurement setup, device parameters, flux-line crosstalk calibration, additional measurement and simulation results for CR gate.
[33] F. Motzoi, J. M. Gambetta, P. Rebentrost, and F. K. Wilhelm, Simple Pulses for Elimination of Leakage in Weakly Nonlinear Qubits, Phys. Rev. Lett. **103**, 110501 (2009).
[34] M. Hatridge, R. Vijay, D. H. Slichter, J. Clarke, and I. Siddiqi, Dispersive magnetometry with a quantum limited SQUID parametric amplifier, Phys. Rev. B **83**, 134501 (2011).
[35] S. S. Roy, A. Shukla, and T. S. Mahesh, NMR implementation of a quantum delayed-choice experiment, Phys. Rev. A **85**, 022109 (2012).
[36] A. Kamal, A. Marblestone, and M. Devoret, Signal-to-pump back action and self-oscillation in double-pump josephson parametric amplifier, Phys. Rev. B **79**, 184301 (2009).
[37] K. W. Murch, S. J. Weber, C. Macklin, and I. Siddiqi, Observing single quantum trajectories of a superconducting quantum bit, Nature (London) **502**, 211 (2013).
[38] T. Roy, S. Kundu, M. Chand, A. M. Vadiraj, A. Ranadive, N. Nehra, M. P. Patankar, J. Aumentado, A. A. Clerk, and R. Vijay, Broadband parametric amplification with impedance engineering: Beyond the gain-bandwidth product, Appl. Phys. Lett. **107**, 262601 (2015).
[39] A. D. Patterson, J. Rahamim, T. Tsunoda, P. A. Spring, S. Jebari, K. Ratter, M. Mergenthaler, G. Tancredi, B. Vlastakis, M. Esposito, and P. J. Leek, Calibration of a cross-resonance two-qubit gate between directly coupled transmons, Phys. Rev. Applied **12**, 064013 (2019).
[40] A. N. Korotkov, Error matrices in quantum process tomography, arXiv:1309.6405.
[41] M. Reed, Entanglement and quantum error correction with superconducting qubits, Ph.D. thesis, Yale University, 2013.
[42] J. M. Chow, Quantum information processing with superconducting qubits, Ph.D. thesis, Yale University, 2010.
[43] N. Sundaresan, I. Lauer, E. Pritchett, E. Magesan, P. Jurcevic, and J. M. Gambetta, Reducing unitary and spectator errors in cross resonance with optimized rotary echoes, Phys. Rev. X Quant. **1**, 020318 (2020).
[44] J. R. Johansson, P. D. Nation, and F. Nori, Qutip: An open-source python framework for the dynamics of open quantum systems, Comput. Phys. Commun. **183**, 1760 (2012).
[45] A. Córcoles, E. Magesan, S. J. Srinivasan, A. W. Cross, M. Steffen, J. M. Gambetta, and J. M. Chow, Demonstration of a quantum error detection code using a square lattice of four superconducting qubits, Nat. Commun. **6**, 6979 (2015).
[46] J. M. Gambetta, J. M. Chow, and M. Steffen, Building logical qubits in a superconducting quantum computing system, npj Quantum Inf. **3**, 2 (2017).